Samples of HNpP did not exhibit photoluminescence at room temperature between 400 and 900 nm. As noted above, we did observe what appears to be photoreduction of HNpP to a green solid upon excitation with 418- and 647-nm Kr^+ laser lines. Introduction of NpO_2^{2+} into the HUP host lattice effectively quenches the characteristic uranyl emission of HUP, analogous to the quenching found by intercalating UO_2^{2+} into HUP.[4]

Samples of NpUP and UNpP have absorption spectra that are a composite of NpO_2^{2+} (450–700 nm and near-IR region) and UO_2^{2+} (400–500 nm) electronic transitions. The electronic spectrum of NpP exhibits two broad, weak absorptions between 400 and 700 nm as well as the characteristic near-infrared Np(VI) absorption. The variations in peak shape in the 900–1200-nm region are noteworthy but have not been further investigated. For none of these species were we able to detect emission from 500 to 900 nm.

Conclusion

Both the HUP and HNpP host lattices intercalate NpO_2^{2+} and UO_2^{2+} ions to yield a family of hydrated, lamellar host lattices. "Cross-intercalation" reactions of UO_2^{2+} into HNpP and of NpO_2^{2+} into HUP demonstrate that host lattice substitution can occur. Both host lattices show a remarkable selectivity for intercalating NpO_2^{2+} over NpO_2^+ under ambient conditions. Vibrational and optical properties of the intercalated solids are derived from the actinyl transitions.

Acknowledgment. Studies at UW—Madison were generously supported by the Office of Naval Research; studies at LANL were supported by the Department of Energy. We thank Dr. D. E. Hobart for his assistance with the preparation of several neptunium solutions and Drs. W. H. Woodruff and S. F. Agnew for their assistance with spectroscopic measurements. P.K.D. wishes to thank Los Alamos National Laboratory for a Graduate Research Assistantship. We thank several reviewers for their helpful comments.

Supplementary Material Available: A table of $1/d^2$ and *hkl* values from powder X-ray diffraction (2 pages). Ordering information is given on any current masthead page.

Contribution from the Central Research and Development Department, Experimental Station E328, E. I. du Pont de Nemours and Company, Inc., Wilmington, Delaware 19898,† Departments of Chemistry and Physics, The Ohio State University, Columbus, Ohio 43210, and Department of Chemistry, Northeastern University, Boston, Massachusetts 02115

Ferromagnetic Behavior in Linear Charge-Transfer Complexes. Structural and Magnetic Characterization of Octamethylferrocene Salts: $[Fe(C_5Me_4H)_2]^{\bullet+}[A]^{\bullet-}$ (A = TCNE, TCNQ)

Joel S. Miller,*[1a] Daniel T. Glatzhofer,[1a,b] Dermot M. O'Hare,[1a] William M. Reiff,*[1c] Animesh Chakraborty,[1b] and Arthur J. Epstein*[1b]

Received January 23, 1989

The reaction of $Fe^{II}(\eta^5\text{-}C_5Me_4H)_2$ with cyano acceptors A [A = TCNE (tetracyanoethylene), TCNQ (7,7,8,8-tetracyano-*p*-quinodimethane), *n*-$C_4(CN)_6$ (*n*-hexacyanobutadiene), $C_6(CN)_6$ [tris(dicyanomethylene)cyclopropane], DDQ (2,3-dichloro-5,6-dicyanobenzoquinone), $TCNQF_4$ (perfluoro-7,7,8,8-tetracyano-*p*-quinodimethane)] results in formation of 1:1 charge-transfer salts of $[Fe^{III}(C_5Me_4H)_2]^{\bullet+}[A]^{\bullet-}$ composition. The TCNE and TCNQ complexes have been structurally characterized. The $[Fe^{III}(C_5Me_4H)_2]^{\bullet+}[TCNE]^{\bullet-}$ salt belongs to the centrosymmetric *Cmca* space group [a = 14.990 (3) Å, b = 11.580 (7) Å, c = 12.503 (4) Å, Z = 4, T = 23 °C, V = 2170 (3) Å^3, R_u = 0.037, R_w = 0.040]. The anion exists as isolated planar $[TCNE]^{\bullet-}$ radicals. The C—C, C—CN, and C≡N bonds are 1.385 (6), 1.426 (4), and 1.135 (5) Å, respectively, and the NC—C—CN, NC—C—C, and N≡C—C angles are 118.7 (4), 120.6 (4), and 179.6 (4)°, respectively. The $[Fe^{III}(C_5Me_4H)_2]^{\bullet+}[TCNQ]^{\bullet-}$ salt belongs to the centrosymmetric $P\bar{1}$ space group [a = 8.636 (1) Å, b = 9.574 (3) Å, c = 10.025 (4) Å, α = 63.77 (3)°, β = 70.22 (2)°, γ = 162.79 (2)°, Z = 1, T = 23 °C, V = 651.6 (3), R_u = 0.052, R_w = 0.054]. The anion exists as isolated planar $[TCNQ]^{\bullet-}$ radicals. The HC—CH, HC—C, C—C(CN)$_2$, C—CN, and C≡N bonds are 1.358, 1.419, 1.405, 1.417, and 1.148 Å, respectively, and the HC—C(H)—C, HC—C—CH, NC—C—CN, NC—C—C, and N≡C—C angles average 121.6, 116.7, 115.6, 122.1, and 178.9°, respectively. The solid-state structure for both salts consists of linear chains of ···$D^{\bullet+}A^{\bullet-}D^{\bullet+}A^{\bullet-}D^{\bullet+}$···. The cation for both salts has a staggered conformation with the Fe asymmetrically bonded to the C_5 ring; i.e., the average Fe–CH and Fe–CMe separations are 2.057 and 2.099 Å, respectively. The Fe–C_5 ring centroid distance is 1.694 Å for the $[TCNE]^{\bullet-}$ salt and is 1.710 Å for the $[TCNQ]^{\bullet-}$ salt. The high-temperature magnetic susceptibility for polycrystalline samples of these complexes can be fit by the Curie–Weiss law, $\chi = C(T - \Theta)^{-1}$, with Θ = +0.5 ± 2.2 K, and μ_{eff} ranges from 2.71 to 3.97 μ_B, suggesting that the polycrystalline samples measured had varying degrees of orientation. The 7.0 K EPR spectrum of the radical cation exhibits an axially symmetric powder pattern with $g_\parallel$ = 4.11 and $g_\perp$ = 1.42, and the EPR parameters are essentially identical with those reported for ferrocenium and decamethylferrocenium. No EPR spectrum is observed at 78 K. Akin to the $[Fe(C_5Me_5)_2]^{\bullet+}$ salts, these salts have ^{57}Fe Mössbauer spectra consistent with complete charge transfer; however, unlike the case for the former complexes, quadrupole splittings of 0.30 and 0.22 mm/s are observed at 4.8 and 298 K, respectively. The absence of strong interionic magnetic coupling for the $[Fe(C_5Me_4H)_2]^{\bullet+}$ salts contrasts with the behavior of the $[Fe(C_5Me_5)_2]^{\bullet+}$ salts.

Introduction

One-dimensional, 1-D, charge-transfer complexes frequently exhibit unusual optical, electrical,[2-4] and, recently, unusual cooperative magnetic properties.[5] For example, the reaction of decamethylferrocene, $Fe(C_5Me_5)_2$, and 7,7,8,8-tetracyano-*p*-quinodimethane, TCNQ, gives three major products of varying stoichiometry, conductivity, and magnetism. Two 1:1 charge-

† Contribution No. 5015.

(1) (a) Du Pont. (b) The Ohio State University. (c) Northeastern University.

(2) See for example: *Extended Linear Chain Compounds*; Miller, J. S., Ed.; Plenum Publisher Corp.: New York, 1982, 1983; Vols. 1-3. Simon, J.; Andre, J. J. *Molecular Semiconductors*; Springer Verlag: New York, 1985.

0020-1669/89/1328-2930$01.50/0

transfer salts can be isolated.[6] The kinetically favored phase comprises 1-D alternating $S = {}^1/_2$ $[Fe(C_5Me_5)_2]^{\bullet+}$ cation donors, D, and $S = {}^1/_2$ $[TCNQ]^{\bullet-}$ anion acceptors, A, i.e., $\cdots D^{\bullet+}A^{\bullet-}D^{\bullet+}A^{\bullet-}\cdots$, and has been shown to have a field-dependent metamagnetic switching from an antiferromagnetic to a high-moment behavior.[5,7] Molecular metamagnetic materials are of fundamental interest; however, the lack of large single crystals and low transition temperature have hampered the detailed study of physical properties. Replacement of $[TCNQ]^{\bullet-}$ with $[TCNE]^{\bullet-}$ (TCNE = tetracyanoethylene) has lead to the similarly structured $[Fe(C_5Me_5)_2]^{\bullet+}[TCNE]^{\bullet-}$, which has been characterized to be a bulk ferromagnet.[5,8,9]

With our observation of ferro- and metamagnetic behavior in 1-D molecular charge-transfer complexes, we purposely sought to elucidate structure–function relationships through modification of the radical cation and independently the radical anion.[5] Herein, the effect of replacing $[Fe(C_5Me_5)_2]^{\bullet+}$ with the lower symmetry $[Fe(C_5Me_4H)_2]^{\bullet+}$ is studied.

The best conceptual framework to view the stabilization of ferromagnetic coupling in molecular based donor/acceptor complexes is based upon the extended McConnell mechanism.[5,10,11] Within this model, the stabilization of ferromagnetic coupling arises from the configurational mixing of a charge-transfer excited state with the ground state. The model predicts that for excitation from a non-half-occupied degenerate HOMO of a donor to an acceptor with a half-filled nondegenerate HOMO, as is the case for $[TCNE]^{\bullet-}$ and $[TCNQ]^{\bullet-}$, ferromagnetic coupling may be stabilized. However, on the basis of the $[Fe(C_5Me_4H)_2]^{\bullet+}$ cation's idealized C_{2h} molecular symmetry, the HOMO cannot be degenerate; thus, this model predicts that $[Fe(C_5Me_4H)_2]^{\bullet+}[A]^{\bullet-}$ (A = TCNE, TCNQ) can only exhibit antiferromagnetic coupling. However, if upon lowering of the D_5 symmetry to C_{2h} the degeneracy of the e_{2g} HOMO is only slightly lifted, then the system would essentially be accidentally degenerate and the extended McConnell model would be consistent with ferromagnetic coupling.[5,10,11] These radical-anion charge-transfer salts provide a means to test some of these concepts. Thus, herein we report complexes based on $[Fe(C_5Me_4H)_2]^{\bullet+}$.

Experimental Section

1,1′,2,2′,3,3′,4,4′-Octamethylferrocene, $Fe(C_5Me_4H)_2$, was prepared from tetramethylcyclopentenone (Aldrich) according to the literature;[12] TCNE (Aldrich) was sublimed prior to use; TCNQ, DDQ, and benzoquinone (Aldrich) were recrystallized prior to use from acetonitrile, chloroform, and chloroform, respectively. $TCNQF_4$,[13a] $C_4(CN)_6$,[13b] and $[n\text{-}Bu_4N][C_3[C(CN)_2]_3]$[13c] were prepared by using literature procedures. All reactions to form charge-transfer salts (except the tetrafluoroborate salt) were performed in a Vacuum Atmospheres Dri-Box under a nitrogen atmosphere. EPR spectra were recorded on an IBM/Bruker ER 200 D-SRC spectrometer. ^1H NMR spectra were recorded on a General Electric QE-30 300-MHz instrument. Magnetic susceptibility data were recorded by using the Faraday technique from ~2–300 K. Infrared spectra were recorded on a Nicolet 7199 Fourier transform spectrometer. Elemental analyses and single-crystal X-ray studies were performed by Oneida Research Services, Inc. (Whitesboro, NY).

$[Fe(C_5Me_4H)_2]^{\bullet+}[BF_4]^-$ was prepared by addition of a solution containing 19 mg (0.84 mmol) of benzoquinone and 307 mg (1.68 mmol) of an 48% aqueous HBF_4 solution in ca. 10 mL of diethyl ether to a stirred solution of 500 mg (1.68 mmol) of $Fe(C_5Me_4H)_2$ in 10 mL of diethyl ether. The light green precipitate that formed was collected by filtration (604 mg) and dissolved in a minimal amount of acetonitrile in a vial that was placed in a closed jar containing a pool of diethyl ether. The diethyl ether vapor was allowed to diffuse into the acetonitrile solution for several days until dark green crystals were apparent. The crystals were filtered out, washed with diethyl ether, and dried under reduced pressure to give 450 mg (70%). A second crop of crystals (80 mg) was obtained by reducing the remaining solution to a small volume and repeating the ether process. Anal. Found (calcd for $C_{18}H_{26}FeBF_4$): C, 56.22 (56.15); H, 6.84 (6.81). The ^1H NMR spectrum shows singlet resonances at −27.25 (CH_3), −36.43 (CH_3), and −444.49 ppm (CH). The half-widths at half-height are 0.69, 0.74, and ~4.5 ppm, respectively. The reduction potential determined via cyclic voltammetry in acetonitrile is 0.07 V vs SCE.

$[Fe(C_5Me_4H)_2]^{\bullet+}[TCNE]^{\bullet-}$ was prepared by adding a solution of 86 mg (0.671 mmol) of tetracyanoethylene in ca. 5 mL of dry acetonitrile to a hot solution of 200 mg (0.671 mmol) of $Fe(C_5Me_4H)_2$ dissolved in ca. 20 mL of dry acetonitrile. The dark solution was allowed to cool slowly to room temperature before being placed in a freezer at −30 °C. The dark needles that formed were collected by filtration and dried under reduced pressure to give 54 mg (19%). Another 94 mg (33%) of the needles was obtained by reduction of the mother liquor to a small volume and cooling as before. Several of the best-formed needles were sent for X-ray analysis. Anal. Found (calcd for $C_{24}H_{26}FeN_4$): C, 67.75 (67.61); H, 6.15 (6.15); N, 13.19 (13.14). IR [Nujol, ν(C≡N)]: 2147 s, 2185 s cm^{-1}.

$[Fe(C_5Me_4H)_2]^{\bullet+}[TCNQ]^{\bullet-}$ was prepared by the above method in 89% yield. Anal. Found (calcd for $C_{30}H_{30}FeN_4$): C, 71.63 (71.72); H, 6.02 (6.02); N, 11.26 (11.15). IR [Nujol, ν(C≡N)]: 2152 m, 2177 s cm^{-1}.

$[Fe(C_5Me_4H)_2]^{\bullet+}[n\text{-}C_4(CN)_6]^{\bullet-}$ was prepared by the above method in 31% yield. Anal. Found (calcd for $C_{28}H_{26}FeN_6$): C, 66.94 (66.94); H, 5.20 (5.22); N, 16.79 (16.73). IR [Nujol, ν(C≡N)]: 2175 m, 2189 s, 2225 w, 2243 w cm^{-1}.

$[Fe(C_5Me_4H)_2]^{\bullet+}[DDQ]^{\bullet-}$ was prepared by the above method in 22% yield. X-ray analysis on several of the best-formed needles showed the crystals to be highly disordered. Anal. Found (calcd for $C_{26}H_{26}FeCl_2N_2O_2$): 58.72 (59.45); H, 4.96 (4.99); N, 5.29 (5.33). IR (Nujol): ν(C≡N) 2206 s, ν(C=O) 1559 m and 1544 s cm^{-1}.

$[Fe(C_5Me_4H)_2]^{\bullet+}[TCNQF_4]^{\bullet-}$ was prepared by the above method in 80% yield. Anal. Found (calcd for $C_{30}H_{26}FeF_4N_4$): C, 62.65 (62.73); H, 4.58 (4.56); N, 9.74 (9.75). IR [Nujol, ν(C≡N)]: 2177 s, 2195 s cm^{-1}.

$[Fe(C_5Me_4H)_2]^{\bullet+}\{C_3[C(CN)_2]_3\}^{\bullet-}$ was prepared by addition of a hot solution of 122 mg (0.260 mmol) of tetra-*n*-butylammonium tris(dicyanomethylene)cyclopropanide in ca. 10 mL of dry acetonitrile to a hot solution of 100 mg (0.260 mmol) of $[Fe(C_5Me_4H)_2]^{\bullet+}[BF_4]^{\bullet-}$ in ca. 7 mL of dry acetonitrile. The solution was reduced somewhat by boiling and allowed to cool to room temperature before being placed in a freezer at −30 °C overnight. The crystals that formed were collected by filtration and dried under reduced pressure to give 88 mg (64%) product. Concentration of the mother liquor and cooling as before gave a second crop (25 mg) of crystals. Anal. Found (calcd for $C_{30}H_{26}FeN_6$): C, 68.42 (68.45); H, 4.98 (4.98); N, 16.08 (15.96). IR [Nujol, ν(C≡N)]: 2198 m, 2208 s cm^{-1}.

^{57}Fe Mössbauer Spectroscopy. Zero-field Mössbauer spectra were determined by using a conventional constant-acceleration spectrometer with a 50-mCi ^{57}Co source electroplated onto the surface and annealed into the body of the 6-μm thick foil of high-purity rhodium in a hydrogen atmosphere. The details of cryogenics, temperature control, etc. have been described previously.[14]

(3) For detailed overview, see the proceedings of the recent series of international conferences: *Synth. Met.* **1987**, *17–19* (Shirakawa, H., Yamabe, T., Yoshino, K., Eds.). *Mol. Cryst. Liq. Cryst.* **1985**, *117–121* (Pecile, C., Zerbi, G., Bozio, R., Girlando, A., Eds.). *J. Phys. Colloq.* **1983**, *44*(C33) (Comes, R., Bernier, P., Andre, J. J., Rouxel, J., Eds.). *Mol. Cryst. Liq. Cryst.* **1981**, *77*, *79*, *82*, *83*, *85*; **1982**, *86* (Epstein, A. J., Conwell, E. M., Eds.). *Chem. Scr.* **1981**, *17* (Carneiro, K., Ed.). *Lect. Notes Phys.* **1979**, *95*, *96* (Bartsic, S., Bjelis, A., Cooper, J. R., Leontic, B. A., Eds.). *Ann. N. Y. Acad. Sci.* **1978**, *313* (Miller, J. S., Epstein, A. J., Eds.).

(4) Epstein, A. J.; Miller, J. S. *Sci. Am.* **1979**, *241*(4), 52–61. Bechgaard, K.; Jerome, D. *Sci. Am.* **1982**, *247*(2), 52–61.

(5) (a) Miller, J. S.; Epstein, A. J.; Reiff, W. M. *Isr. J. Chem.* **1987**, *27*, 363–373. (b) Miller, J. S.; Epstein, A. J.; Reiff, W. M. *Chem. Rev.* **1988**, *88*, 201. (c) Miller, J. S.; Epstein, A. J.; Reiff, W. M. *Acc. Chem. Res.* **1988**, *21*, 114. (d) Miller, J. S.; Epstein, A. J.; Reiff, W. M. *Science* **1988**, *240*, 40–47.

(6) Miller, J. S.; Reiff, W. M.; Zhang, J. H.; Preston, L. D.; Reis, A. H., Jr.; Gebert, E.; Extine, M.; Troup, J.; Dixon, D. A.; Epstein, A. J.; Ward, M. D. *J. Phys. Chem.* **1987**, *91*, 4344–4360.

(7) Candela, G. A.; Swartzendruber, L.; Miller, J. S.; Rice, M. J. *J. Am. Chem. Soc.* **1979**, *101*, 2755–2756.

(8) (a) Miller, J. S.; Calabrese, J. C.; Bigelow, R. W.; Epstein, A. J.; Zhang, R. W.; Reiff, W. M. *J. Chem. Soc., Chem. Commun.* **1986**, 1026–1028. (b) Miller, J. S.; Calabrese, J. C.; Rommelmann, H.; Chittapeddi, S.; Zhang, J. H.; Reiff, W. M.; Epstein, A. J. *J. Am. Chem. Soc.* **1987**, *109*, 769–781.

(9) Chittapeddi, S.; Cromack, K. R.; Miller, J. S.; Epstein, A. J. *Phys. Rev. Lett.* **1987**, *22*, 2695.

(10) McConnell, H. M. *Proc. Robert A. Welch Found. Conf. Chem. Res.* **1967**, *11*, 144.

(11) Miller, J. S.; Epstein, A. J. *J. Am. Chem. Soc.* **1987**, *109*, 3850–3855.

(12) Kohler, F. H.; Doll, K. H. *Z. Naturforsch.* **1982**, *87B*, 144–150.

(13) (a) Wheland, R. C.; Martin, E. L. *J. Org. Chem.* **1975**, *40*, 3101. (b) Webster, O. *J. Am. Chem. Soc.* **1964**, *86*, 2898. (c) Fukunaga, T. *J. Am. Chem. Soc.* **1976**, *98*, 610. Fukanaga, T. *J. Am. Chem. Soc.* **1976**, *98*, 611.

(14) Cheng, C.; Reiff, W. M. *Inorg. Chem.* **1977**, *16*, 2097.

Table I. Crystallographic Data for $[Fe(C_5Me_4H)_2]^{+}[A]^{-}$ (A = TCNE, TCNQ)

	anion, $[A]^{-}$	
	$[TCNE]^{-}$	$[TCNQ]^{-}$
formula	$C_{24}H_{26}N_4Fe$	$C_{30}H_{30}N_4Fe$
fw	426.35	502.45
space group	*Cmca* (No. 64)	$P\bar{1}$ (No. 2)
a, Å	14.990 (3)	8.636 (1)
b, Å	11.580 (7)	9.574 (3)
c, Å	12.503 (4)	10.025 (4)
α, deg	90	63.77 (3)
β, deg	90	70.22 (2)
γ, deg	90	62.79 (2)
V, Å^3	2170 (3)	651.6 (3)
Z	4	1
ρ(calc), g cm^{-3}	1.30	1.28
cryst dimens, mm	0.21 × 0.38 × 0.78	0.18 × 0.20 × 0.68
radiation wavelength (λ), Å	0.710 73	1.541 84
abs coeff (μ), cm^{-1}	7.1	48.3
temp, °C	23	23
$R_u(F_o^2)$	0.037	0.054
$R_w(F_o^2)$	0.040	0.052

X-ray Structure Determination

X-ray Data Collection. $[Fe(C_5Me_4H)_2]^{+}[TCNE]^{-}$ crystals were grown by slow cooling of a saturated acetonitrile solution. Cell constants and an orientation matrix for the data collection were obtained from least-squares refinement using the angles of 16 reflections in the range $12 < \theta < 18°$. Systematic absences (hkl, $h + k = 2n + 1$; $h0l$; $l = 2n + 1$; $hk0$, $h, k = 2n + 1$) and subsequent least-squares refinement determined the space group to be *Cmca* (No. 64). During data collection the intensity of three representative reflections were monitored as a check on crystal stability. There was loss of intensity during data collection, and an isotropic decay correction was applied. The correction factors on *I* ranged from 0.913 to 1.037. Equivalent reflections were merged, and only those for which $(F_o)^2 \geq 3\sigma(F_o)^2$ were included in the refinement, where $\sigma(F_o)^2$ is the standard deviation based on counting statistics. Data were also corrected for Lorentz and polarization factors. No absorption correction was made. Crystallographic details are presented in Tables I and S1 (supplementary material).

$[Fe(C_5Me_4H)_2]^{+}[TCNQ]^{-}$ crystals were grown by slow cooling of a saturated acetonitrile solution. Cell constants and an orientation matrix for the data collection were obtained from least-squares refinement using the setting angles of 10 reflections in the range $10 < \theta < 22°$. Systematic absences were not observed, and the space group was found to be $P\bar{1}$ (No 2). During data collection the intensity of three representative reflections were monitored as a check on crystal stability. There was loss of intensity during data collection, and an isotropic decay correction was applied. The correction factors on I ranged from 1.002 to 1.163. Equivalent reflections were merged, and only those for which $F_o^2 > 2\sigma F_o^2$ were included in the refinement, where $\sigma(F_o)^2$ is the standard deviation based on counting statistics. Data were also corrected for Lorentz and polarization factors. No absorption correction was made. Crystallographic details are presented in Tables I and S1 (supplementary material).

Structure Solution and Refinement. $[Fe(C_5Me_4H)_2]^{+}[TCNE]^{-}$. The structure was solved by direct methods. Nine atoms were located from an *E* map prepared from the phase set with probability statistics. The Fe atom and TCNE were located on the special positions $\langle {}^1/_2, 0, 0\rangle$ and $\langle 0, 0, 0\rangle$, respectively, with site symmetry $2/m$. The remaining atoms were located in succeeding difference Fourier syntheses. Hydrogen atoms were added to the structure factor calculations at their calculated positions, but their positions were not refined.

$[Fe(C_5Me_4H)_2]^{+}[TCNQ]^{-}$. The structure was solved by the Patterson heavy-atom method, which revealed the Fe atom position. The remaining atoms were located in succeeding difference Fourier syntheses. Hydrogen atoms were added to the structure factor calculations at their calculated positions, but their positions were not refined.

For both complexes the neutral-atom scattering factors were taken from Cromer and Waber.[15] Anomalous dispersion effects were included in F_c;[16] the values for f' and f'' were those of Cromer.[17] All calculations were performed on a VAX-11/750 computer using the SDP-PLUS package.[18]

Table II. Positional Parameters and Their Estimated Standard Deviations for $[Fe(C_5Me_4H)_2]^{+}[TCNE]^{-}$

atom	*x*	*y*	*z*	B_{ISO},[a] Å^2
Fe	0.500	0.000	0.000	2.82 (1)
N	−0.1468 (2)	0.0876 (3)	−0.1379 (3)	6.50 (7)
C1	0.500	0.0937 (3)	0.1393 (3)	3.65 (7)
C2	0.4229 (2)	0.1238 (2)	0.0795 (2)	3.61 (5)
C3	0.4525 (2)	0.1700 (2)	−0.0194 (2)	3.59 (5)
C4	0.3284 (2)	0.1100 (3)	0.1168 (3)	5.63 (8)
C5	0.3937 (2)	0.2143 (3)	−0.1073 (3)	5.28 (7)
C6	−0.0818 (2)	0.0623 (3)	−0.0977 (3)	4.75 (7)
C7	0.000	0.0301 (3)	−0.0479 (4)	4.50 (9)
H1	0.500	0.059	0.210	5.0*
H4a	0.319	0.156	0.181	5.0*
H4b	0.288	0.137	0.061	5.0*
H4c	0.316	0.030	0.132	5.0*
H5a	0.357	0.277	−0.081	5.0*
H5b	0.430	0.241	−0.166	5.0*
H5c	0.355	0.152	−0.132	5.0*

[a] Asterisks indicate values for atoms refined isotropically. Anisotropically refined atoms are given in the form of the isotropic equivalent displacement parameter defined as $(4/3)[a^2B(1,1) + b^2B(2,2) + c^2B(3,3) + ab(\cos\gamma)B(1,2) + ac(\cos\beta)B(1,3) + bc(\cos\alpha)B(2,3)]$.

Table III. Bond Distances (Å) for $[Fe(C_5Me_4H)_2]^{+}[TCNE]^{-}$

Fe–C1	2.052 (4)	C2–C4	1.499 (4)
Fe–C2	2.093 (3)	C3–C5	1.500 (4)
Fe–C3	2.107 (2)	N–C6	1.135 (5)
C1–C2	1.420 (3)	C6–C7	1.426 (4)
C2–C3	1.419 (4)	C7–C7	1.385 (6)
C3–C3	1.424 (3)		

Results and Discussion

Chemistry. Octamethylferrocene is a yellow crystalline material with an oxidation potential of 0.07 V (vs SCE) intermediate between those of ferrocene (0.41 V vs SCE) and decamethylferrocene (−0.12 V). As a consequence, complete electron transfer occurs upon reaction with strong acceptors such as TCNE, TCNQ, *n*-$C_4(CN)_6$, DDQ, and $\{C_3[C(CN)_2]_3\}^{-}$. These darkly colored 1:1 electron-transfer salts exhibit ν_{CN} vibrational spectra and magnetic susceptibility characteristic of the radical anion.[19]

Crystal Structures of $[Fe(C_5Me_4H)_2]^{+}[A]^{-}$ (A = TCNE, TCNQ). $[Fe(C_5Me_4H)_2]^{+}[TCNE]^{-}$ crystallizes in the orthorhombic *Cmca* space group. The atom labeling and a stereoview of the unit cell can be found in Figures 1 and 2, respectively. The atomic coordinates and bond distances are given in Tables II and III, respectively. Tables of bond angles, least-square planes, and thermal parameters are found in Tables S2–S4, respectively (supplementary material).

$[Fe(C_5Me_4H)_2]^{+}[TCNQ]^{-}$ crystallizes in the centrosymmetric triclinic $P\bar{1}$ space group. The atom labeling and a stereoview of the unit cell can be found in Figures 3 and 4, respectively. The atomic coordinates and bond distances are given in Tables IV and V, respectively. Tables bond angles, least-square planes, and thermal parameters are found in Tables S5–S7, respectively (supplementary material).

$[Fe(C_5Me_4H)_2]^{+}$. The cations for both the $[TCNE]^{-}$ and $[TCNQ]^{-}$ salts are in a staggered conformation with distances essentially equivalent to those previously reported for $[Fe(C_5Me_5)_2]^{+}$ cations.[8b] For the $[TCNE]^{-}$ salt the Fe–C, C–C, and C–Me separations range 2.052 (4)–2.107 (2), 1.419 (4)–1.424 (4), and 1.499 (4)–1.500 (4), respectively, and average 2.084, 1.427, and 1.499 Å, respectively. The ring C–H distance is 0.970 (4) Å, while the Fe–C_5-ring centroid distance is 1.694 Å. As pointed out by an astute reviewer, the Fe–C(H) distance {2.052

(15) Cromer, D. T.; Waber, J. T. *International Tables for X-Ray Crystallography*; The Kynoch Press: Birmingham, England, 1974; Vol. IV, Table 2.2B.
(16) Ibers, J. A.; Hamilton, W. C. *Acta Crystallogr.* **1964**, *17*, 781.
(17) Cromer, D. T.; Waber, J. T. *International Tables for X-Ray Crystallography*; The Kynoch Press: Birmingham, England, 1974; Vol. IV, Table 2.3.1.
(18) Frenz, B. A. The Enraf-Nonius CAD 4 SDP-A Real Time System for Concurrent X-Ray Data Collection and Crystal Structure Determination. In *Computing in Crystallography*; Schenk, H., Olthof-Hazelkamp, R., Vankonigsveld, H., Bassi, G. C., Eds.; Delft University Press: Delft, Holland, 1978; pp 64–71.
(19) Miller, J. S.; Dixon, D. A. *Science* **1987**, *235*, 871.

Table IV. Positional Parameters and Their Estimated Standard Deviations for $[Fe(C_5Me_4H)_2]^{+}[TCNQ]^{-}$

atom	x	y	z	B_{ISO},[a] Å^2
Fe	0.0000	0.0000	0.0000	3.22 (1)
N28	0.3991 (4)	0.1149 (4)	0.2531 (4)	7.9 (1)
N29	0.6233 (4)	0.3186 (4)	0.4186 (4)	8.1 (1)
C1	−0.0767 (4)	−0.2065 (3)	0.1235 (3)	4.87 (8)
C2	0.1103 (4)	−0.2629 (3)	0.0868 (3)	4.30 (7)
C3	0.1701 (3)	−0.1956 (3)	0.1519 (3)	4.00 (7)
C4	0.0229 (4)	−0.0976 (3)	0.2279 (3)	4.28 (7)
C5	−0.1302 (4)	−0.1033 (4)	0.2101 (4)	4.94 (9)
C6	−0.1966 (5)	−0.2503 (5)	0.0848 (5)	8.8 (1)
C7	0.2256 (6)	−0.3760 (4)	−0.0023 (4)	7.4 (1)
C8	0.3588 (4)	−0.2265 (5)	0.1446 (4)	6.4 (1)
C9	0.0259 (6)	−0.0082 (4)	0.3167 (4)	7.2 (1)
C28	0.3747 (4)	0.1992 (4)	0.3173 (4)	5.6 (1)
C29	0.4983 (4)	0.3128 (4)	0.4083 (4)	5.8 (1)
C30	0.3442 (4)	0.3061 (4)	0.3928 (4)	4.87 (8)
C31	0.1733 (4)	0.4030 (3)	0.4454 (3)	4.30 (8)
C32	0.1448 (4)	0.5099 (4)	0.5208 (3)	4.57 (8)
C33	−0.0203 (4)	0.6021 (3)	0.5736 (3)	4.60 (8)
H5	−0.251	−0.046	0.250	5.0*
H6a	−0.128	−0.322	0.025	5.0*
H6b	−0.260	−0.308	0.177	5.0*
H6c	−0.280	−0.149	0.028	5.0*
H7a	0.348	−0.395	−0.011	5.0*
H7b	0.208	−0.482	0.048	5.0*
H7c	0.195	−0.325	−0.102	5.0*
H8a	0.363	−0.166	0.198	5.0*
H8b	0.422	−0.345	0.191	5.0*
H8c	0.414	−0.189	0.040	5.0*
H9a	−0.094	0.050	0.357	5.0*
H9b	0.091	−0.089	0.399	5.0*
H9c	0.083	0.072	0.251	5.0*
H32	0.246	0.517	0.535	5.0*
H33	−0.034	0.673	0.625	5.0*

[a] Asterisks indicate values for atoms refined isotropically. Anisotropically refined atoms are given in the form of the isotropic equivalent displacement parameter defined as $(4/3)[a^2B(1,1) + b^2B(2,2) + c^2B(3,3) + ab(\cos\gamma)B(1,2) + ac(\cos\beta)B(1,3) + bc(\cos\alpha)B(2,3)]$.

Table V. Bond Distances (Å) for $[Fe(C_5Me_4H)_2]^{+}[TCNQ]^{-}$

Fe–C1	2.089 (3)	C4–C9	1.495 (7)
Fe–C2	2.106 (2)	C5–H5	0.971 (3)
Fe–C3	2.112 (2)	N28–C28	1.150 (7)
Fe–C4	2.093 (3)	N29–C29	1.146 (6)
Fe–C5	2.062 (3)	C28–C30	1.411 (6)
C1–C2	1.418 (4)	C29–C30	1.423 (6)
C1–C5	1.419 (6)	C30–C31	1.405 (4)
C2–C3	1.419 (6)	C31–C32	1.417 (6)
C3–C4	1.401 (4)	C31–C33	1.422 (5)
C4–C5	1.421 (6)	C32–C33	1.358 (4)
C1–C6	1.488 (7)	C32–H32	0.971 (4)
C2–C7	1.492 (5)	C33–H33	0.971 (4)
C3–C8	1.498 (5)		

(4) Å for the $[TCNE]^{-}$ salt; 2.062 (3) Å for the $[TCNQ]^{-}$ salt)] is substantially shorter than the Fe–C(Me) distance [2.093 (3) and 2.107 (2) Å for the $[TCNE]^{-}$ salt; 2.089 (3)–2.112 (2) Å for the $[TCNQ]^{-}$ salt)]. This suggests that the Fe asymmetrically bonds to the C_5 ring. The average Fe–CH and Fe–CMe distances are 2.057 and 2.099 Å, respectively.

The $[TCNQ]^{-}$ salt has Fe–C, C–C, and C–Me separations ranging 2.062 (3)–2.112 (2), 1.401 (4)–1.421 (6), and 1.488 (7)–1.498 (5) and averaging 2.092, 1.416, and 1.493 Å, respectively. The ring C–H distance is 0.971 (3) Å, while the Fe–C_5 ring centroid distance is 1.710 Å.

The average Fe–C, C–C, and C–Me distances are 2.088, 1.422, and 1.496 Å, respectively. Like those in decamethylferrocene,[8b] the C–C and C–Me distances are essentially equivalent to those in $Fe^{II}(C_5Me_4H)_2$[20] and the Fe–C distance is 0.034 Å shorter than that in $Fe(C_5Me_4H)_2$.[20]

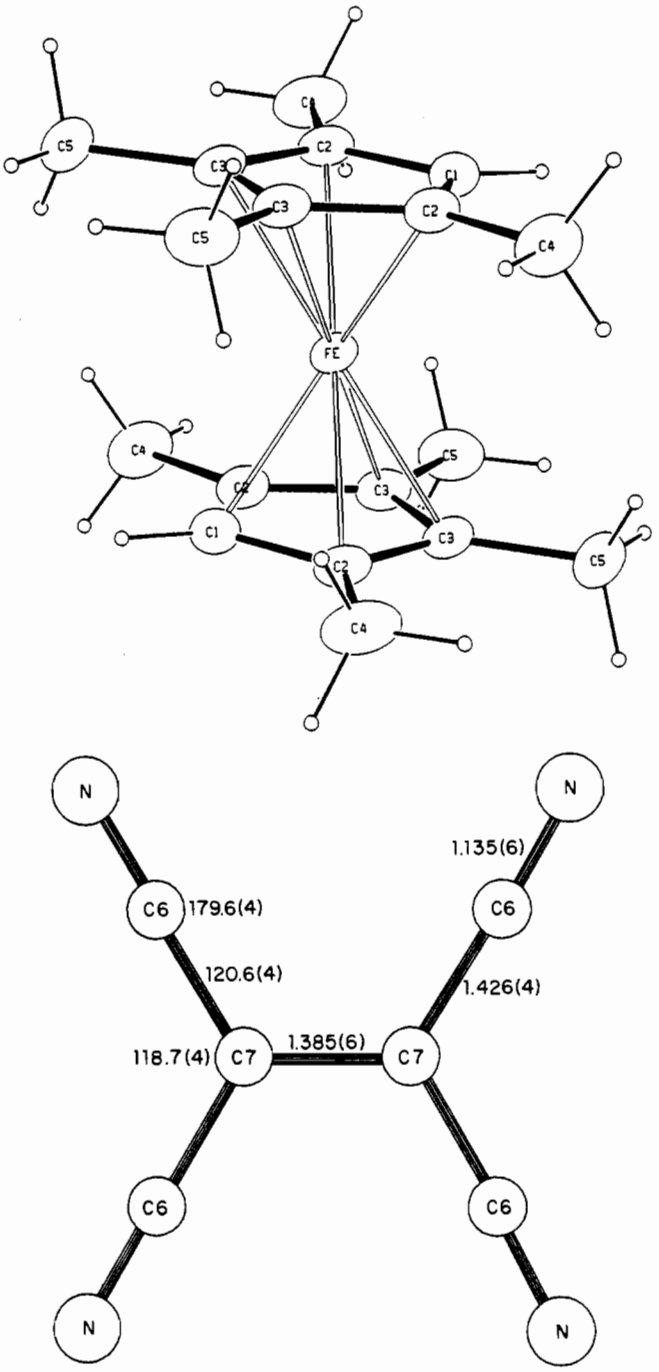

Figure 1. Atom labeling for $[Fe(C_5Me_4H)_2]^{+}[TCNE]^{-}$.

$[TCNE]^{-}$. The planar radical anion lies between essentially parallel C_5Me_4H groups, which do not distort the ion. The distances and angles are very close to the values reported previously for the anion in $[Fe(C_5Me_5)_2]^{+}[TCNE]^{-}$.[8b] The central C—C, C—CN and C≡N distances are 1.385 (6), 1.426 (4), and 1.135 (5) Å, respectively. The NC—C—CN, NC—C—C, and N≡C—C angles are 118.7 (4), 120.6 (4), and 179.6 (4)°, respectively.

$[TCNQ]^{-}$. The planar radical anion lies between essentially parallel C_5Me_4H groups, which do not distort the ion. The distances and angles are very close to those previously reported for $[TCNQ]^{-}$.[6,21] The HC—CH, HC—$CC(CN)_2$, C—$C(CN)_2$, C—CN, and C≡N distances average 1.358, 1.419, 1.405, 1.417, and 1.148 Å, respectively. The HC—C(H)—C, HC—C—CH, NC—C—CN, NC—C—C, and N≡C—C angles average 121.6, 116.7, 115.6, 122.1, and 178.9°, respectively.

(20) Struchkov, Yu. T.; Andrianov, V. G.; Sal'nikova, T. N.; Lyatifov, I. R.; Materikova, R. B. *J. Organomet. Chem.* **1978**, *145*, 218–223.

(21) Flandrois, S.; Chasseau, D. *Acta Crystallogr.* **1977**, *B33*, 2744. Herbstein, F. H. *Perspect. Struct. Chem.* **1971**, *4*, 166–395. Shibaeva, R. R.; Atovmyan, L. U. *J Struct. Chem.* **1972**, *13*, 514–551.

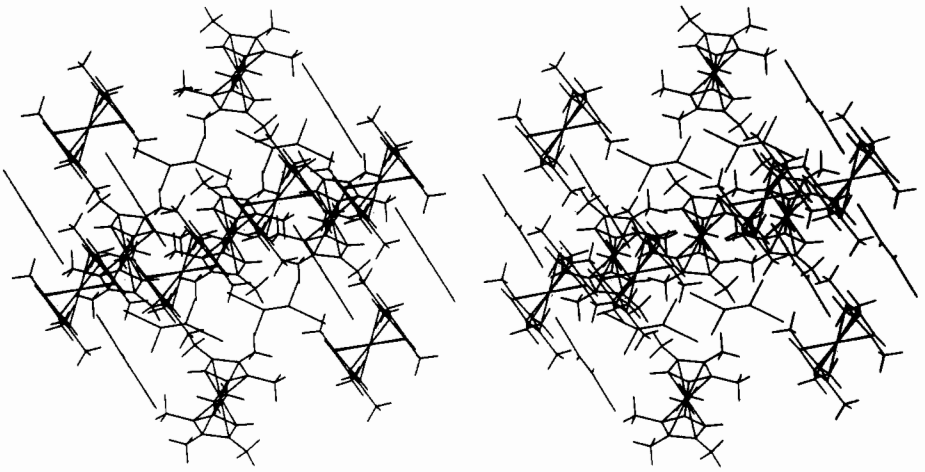

Figure 2. Stereoview of the unit cell for $[Fe(C_5Me_4H)_2]^{\bullet+}[TCNE]^{\bullet-}$.

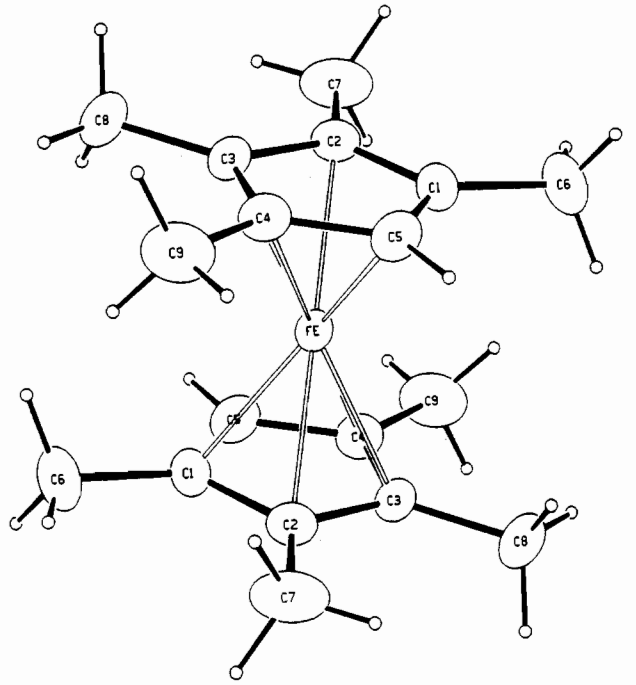

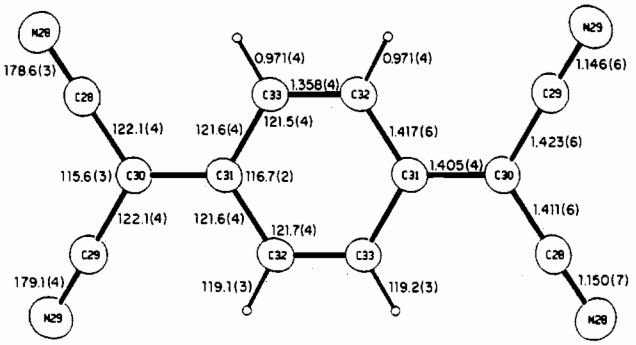

Figure 3. Atom labeling for $[Fe(C_5Me_4H)_2]^{\bullet+}[TCNQ]^{\bullet-}$.

Solid-State Structures. Like the structures found for the ferromagnet $[Fe(C_5Me_5)_2]^{\bullet+}[TCNE]^{\bullet-}$, metamagnet $[Fe(C_5Me_5)_2]^{\bullet+}[TCNQ]^{\bullet-}$, and the $[DDQ]^{\bullet-}$, $[C_4(CN)_6]^{\bullet-}$, and $[C_6(CN)_6]^{\bullet-}$ salts of $[Fe(C_5Me_5)_2]^{\bullet+}$,[5a] those of the $[TCNE]^{\bullet-}$ and $[TCNQ]^{\bullet-}$ salts of $[Fe(C_5Me_4H)_2]^{\bullet+}$ have a linear chain $\cdots D^{\bullet+}A^{\bullet-}D^{\bullet+}A^{\bullet-}D^{\bullet+}A^{\bullet-}\cdots$ structure in the solid state.

Since cooperative magnetic phenomena are bulk properties, the interchain as well as the intrachain interactions are of fundamental importance. This information is important to understand the spin–spin interactions, which should dominate the magnetic behavior, especially in view of the structural information previously reported for the ferromagnetically coupled $[TCNE]^{\bullet-}$[8b] and antiferromagnetically coupled $[TCNQ]^{\bullet-}$[6] salts of $[Fe(C_5Me_5)_2]^{\bullet+}$. Thus, it is important to discuss the inter- and intrachain Fe–Fe, Fe–N, and N–N separations.

$[Fe(C_5Me_4H)_2]^{\bullet+}[TCNE]^{\bullet-}$. The unit cell comprises three unique interchain interactions, namely A–B, A–C, and A–D (Figure 5). Chains A–C are essentially in-registry, whereas chains A–B and A–D are out-of-registry (Figure 6).

The intrachain Fe–N interactions (Figure 6a) are 5.534 and 7.357 Å and average 6.446 Å. This is 0.42 Å longer than that observed for the monoclinic phase of $[Fe(C_5Me_5)_2]^{\bullet+}[TCNE]^{\bullet-}$. Although the shortest distance is shorter than that observed for $[Fe(C_5Me_5)_2]^{\bullet+}[TCNE]^{\bullet-}$, canting of the ions enables several of the Fe···N separations to be longer. The N···N separation for the in-registry A–C chains is 4.173 Å, which is 0.55 Å shorter than that observed for $[Fe(C_5Me_5)_2]^{\bullet+}[TCNE]^{\bullet-}$.[8b] As an additional consequence of the canting, the in-registry Fe···Fe separation of 9.760 Å is 1 Å longer than the comparable distances observed for $[Fe(C_5Me_5)_2]^{\bullet+}[TCNE]^{\bullet-}$. In contrast, canting enables the average out-of-registry Fe···Fe separations to be shorter by 0.75 Å. In general, the structures of $[Fe(C_5Me_5)_2]^{\bullet+}[TCNE]^{\bullet-}$ and $[Fe(C_5Me_4H)_2]^{\bullet+}[TCNE]^{\bullet-}$ are comparable with canting of the ions for the latter structure, altering some of the relative atomic contacts by as much as 1 Å. These differences are significant enough to suggest that if substantial differences in the physical properties were observed, they could be explained by structural differences.

$[Fe(C_5Me_4H)_2]^{\bullet+}[TCNQ]^{\bullet-}$. The unit cell comprises three unique interchain interactions, namely E–F, E–G, and F–G (Figure 7). Chains E–F are essentially in-registry, whereas chains E–G and F–G are out-of-registry (Figure 8).

The four intrachain Fe···N interactions (6.919, 6.937, 7.093, and 7.094 Å) are essentially equivalent (Figure 8a) and average 7.010 Å. This is 0.21 Å shorter than that observed for the metamagnetic phase of $[Fe(C_5Me_5)_2]^{\bullet+}[TCNQ]^{\bullet-}$.[6] However, four Fe···N separations are shorter than 6.9 Å and the other four are longer than 7.094 Å. The shortest interchain Fe···Fe and N···N separations for the in-registry E–F chains are 8.636 and 3.895 Å, respectively. The intrachain Fe···Fe separation of 10.360 Å is essentially equivalent (<0.2 Å shorter) to those in the comparable $[Fe(C_5Me_5)_2]^{\bullet+}[TCNE]^{\bullet-}$[6] and $[Fe(C_5Me_5)_2]^{\bullet+}[TCNQ]^{\bullet-}$[8b] salts but 1 Å shorter than that observed for $[Fe(C_5Me_4H)_2]^{\bullet+}[TCNE]^{\bullet-}$. For the out-of-registry chain interactions the Fe···Fe separations are 9.520, 9.574, 10.025, and 10.793 Å. In contrast, the out-of-registry Fe···N spacings are 4.786, 5.522, and 5.602 Å. The shortest out-of-registry N···N separations of 4.040, 5.009, are 6.718 Å are longer than the shortest in-registry separation of 3.895 Å. In general, the structures of $[Fe(C_5Me_5)_2]^{\bullet+}[TCNQ]^{\bullet-}$ and $[Fe(C_5Me_4H)_2]^{\bullet+}[TCNQ]^{\bullet-}$ are very comparable, suggesting that, all other factors being equal, similar properties should be anticipated.

Electronic Structure. It is important to establish the electronic configuration of the octamethylferrocenium cation. One physical probe is the EPR spectrum of the radical cation. The EPR spectra

Table VI. Electron Paramagnetic Resonance Data for Ferrocenium Ions

compd	T, K	$g_\parallel$	$g_\perp$	Δg^b	$\langle g\rangle^c$	$k_\parallel$	ζ/δ^d	δ	$\langle\mu_{eff}\rangle^e$	solv^f	ref
$[Fe(C_5H_5)_2]^{\bullet+}[I_3]^-$	20	4.35	1.26	3.09	2.71	0.75	1.23	266	2.35	DMF	22b,c
$[Fe(C_5H_5)(C_5H_4Me)]^{\bullet+}[I_3]^-$	20	4.17	1.47	2.70	2.69	0.80	0.92	356	2.33	DMF	22b,c
$[Fe(C_5H_4Me)_2]^{\bullet+}[I_3]^-$	20	3.83	1.67	2.16	2.60	0.84	0.65	505	2.25	DMF	22b,c
$[Fe(C_5H_4Me)_2]^{\bullet+}[PF_6]^-$	12	4.00	1.92	2.08	2.79				2.42	*a*	22a
$[Fe(C_5H_4)_2(CH_2)_3]^{\bullet+}[PF_6]^-$	12	3.86	1.81	2.05	2.67				2.31	*a*	22a
$[Fe(C_5H_5)(C_5Me_5)]^{\bullet+}[BF_4]^-$	5	4.36	1.24	3.12	2.71	0.71	1.27	259	2.35	*g*	23
$[Fe(C_5Me_5)_2]^{\bullet+}[PF_6]^-$	12	4.43	1.35	3.08	2.78	0.82	1.09	301	2.41	*a*	22a
$[Fe(C_5Me_4H)_2]^{\bullet+}[BF_4]^-$	7	4.11	1.42	2.69	2.64	0.76	0.97	338	2.29	*g*	this work

[a] EPR spectra run on microcrystalline samples. [b] g-tensor anisotropy defined as $\Delta g = g_\parallel - g_\perp$. [c] $\langle g\rangle = [(g_\parallel^2 + 2g_\perp^2)/3]^{1/2}$. [d] Spin–orbit coupling constant taken as 328 cm^{-1}.[22a] [e] $\langle\mu_{eff}\rangle = \langle g\rangle[S(S+1)]^{1/2}$. [f] *N*,*N*-Dimethylformamide. [g] CH_2Cl_2/2-methyltetrahydrofuran.

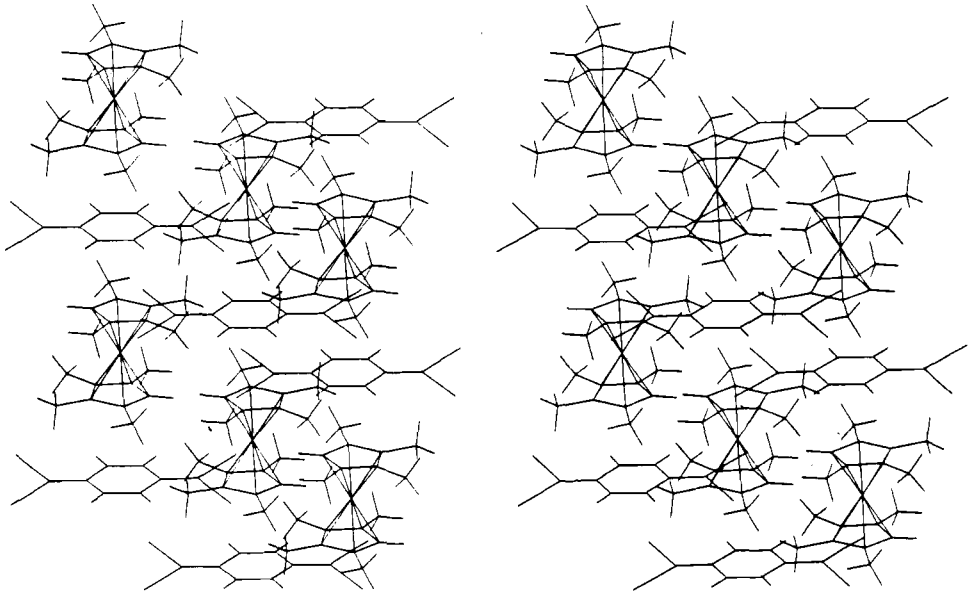

Figure 4. Stereoview of the unit cell for $[Fe(C_5Me_4H)_2]^{\bullet+}[TCNQ]^{\bullet-}$.

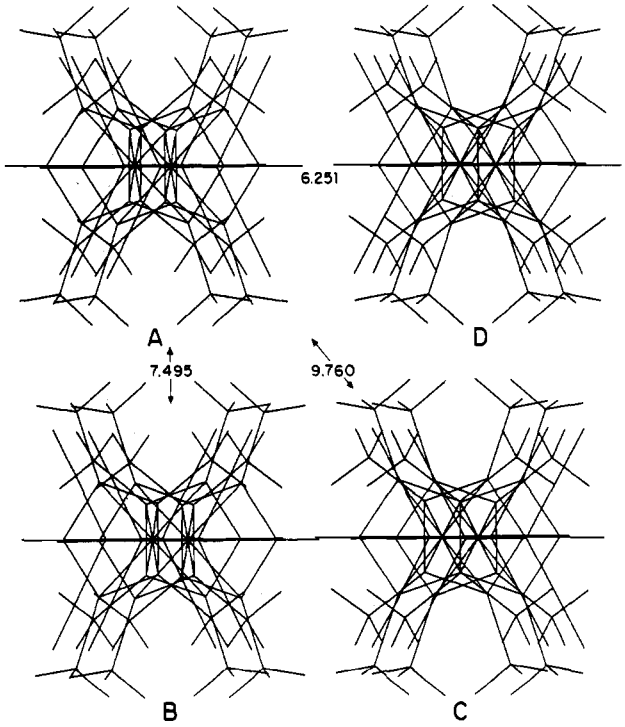

Figure 5. View normal to chains, showing the four unique chains A, B, C, and D for $[Fe(C_5Me_4H)_2]^{\bullet+}[TCNE]^{\bullet-}$.

of ferrocenium cations are only observable in dilute diamagnetic glasses at liquid-helium temperatures.[22b,c] The d^5 $a_{1g}{}^2e_{2g}{}^3$ electronic configuration of ferrocenium cations results in a $^2E_{2g}$ ground state in D_5 point symmetry. The ^2E ground state allows for rapid spin–lattic relaxation and highly anisotropic g tensors. Prins has derived approximate g-value expressions appropriate for ferrocenium cations:[22b]

$$g_z = g_\parallel = 2 + 4k_\parallel[-(\xi/\delta)/(1 + \xi^2/\delta^2)^{1/2}]$$

$$g_x = g_y = g_\perp = 2/(1 + \xi^2/\delta^2)^{1/2}$$

where ξ is the spin–orbit coupling (ca. 328 cm^{-1} for Fe^{3+} [22a]), $k_\parallel$ is the orbital reduction factor, and δ is the one-electron orbital-energy splitting, which scales the distortion from D_5 symmetry.[22]

The g values for ferrocenium cations are generally very far from the free-electron g values and are dominated by contributions from orbital angular momentum.[22] However, for ferrocenium systems with lower symmetry, and larger distortion parameters, δ, the g-tensor anisotropy, Δg, decreases and approaches 2.0. Thus, EPR spectroscopy is a valuable probe to the distortions of ^2E ground states.

The EPR spectrum of $[Fe(C_5Me_4H)_2]^{\bullet+}[BF_4]^-$ was measured in CH_2Cl_2/2-methyltetrahydrofuran at 7 K and shows an axially symmetrical powder pattern characterized by $g_\parallel = 4.11$ and $g_\perp = 1.42$ (Figure 9). Like the case of $[Fe(C_5H_5)_2]^{\bullet+}$ and $[Fe(C_5Me_5)_2]^{\bullet+}$, a spectrum is not observed at 77 K. These values are comparable to those reported for other ferrocene cations (Table VI). The g anisotropy, $\Delta g = g_\parallel - g_\perp$, of 2.68 is significantly lower than 3.08 ± 0.01 found for both ferrocenium and decamethylferrocenium cations and reflects the inherently lower C_{2h} symmetry for $[Fe(C_5Me_4H)_2]^{\bullet+}$ vs D_{5h} for $[Fe(C_5Me_5)_2]^{\bullet+}$ (Table VI).

The one-electron orbital-energy splitting, δ, varies extensively and is strongly dependent on the degree of substitution. The $k_\parallel$ parameter, which reflects the extent of metal–ligand mixing and the strength of the vibronic coupling, is small. Nonetheless, δ for $[Fe(C_5Me_4H)_2]^{\bullet+}$ (338 cm^{-1}) is comparable to those reported for $[Fe(C_5Me_5)_2]^{\bullet+}$ (301 cm^{-1}), $[Fe(C_5H_5)_2]^{\bullet+}$ (266 cm^{-1}),[21] and

(22) (a) Duggan, D. M.; Hendrickson, D. N. *Inorg. Chem.* **1975**, *14*, 955–970. (b) Warren, K. D. *Struct. Bonding (Berlin)* **1976**, *45*, 45. (c) Prins, R. *Mol. Phys.* **1970**, *19*, 602–620. (d) Ammeter, J. H. *J. Magn. Reson.* **1978**, *30*, 299–325.

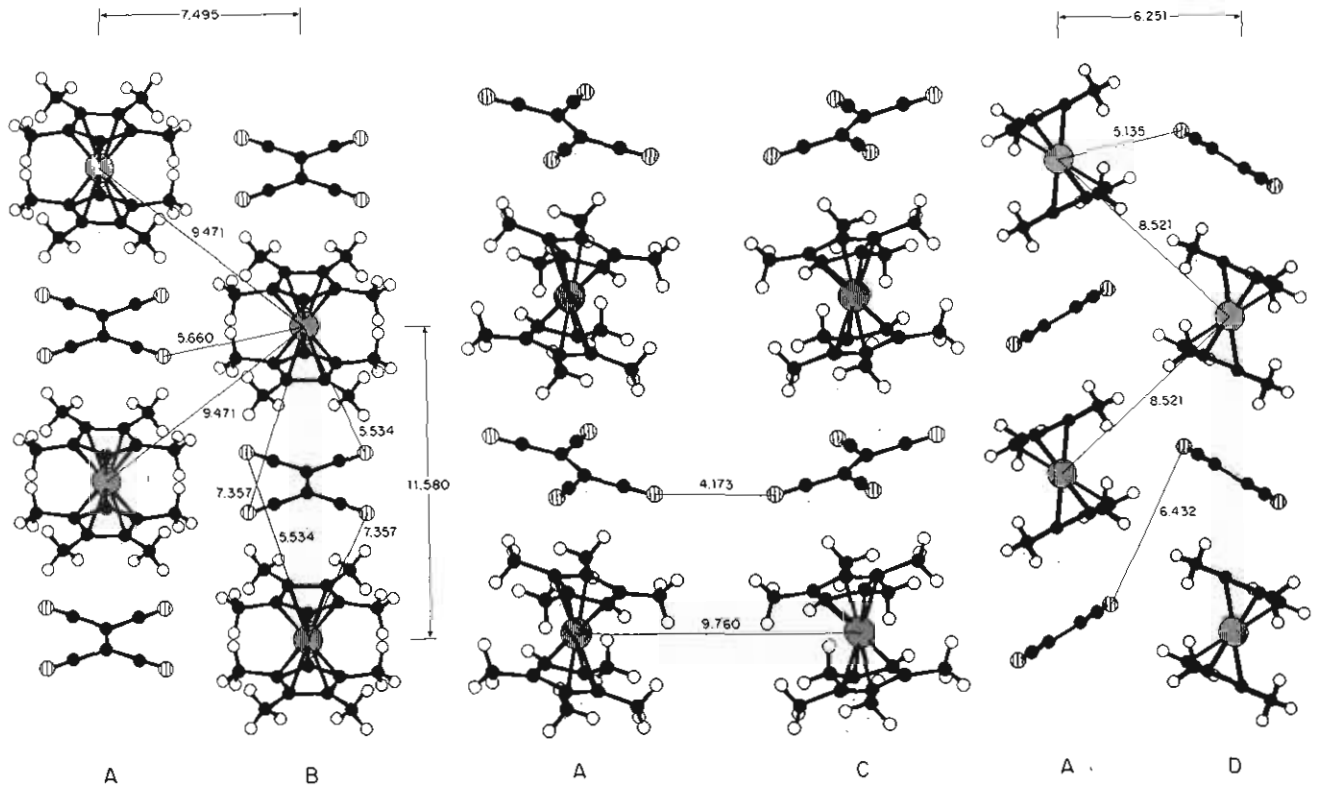

Figure 6. Out-of-registry interactions between chains A–B (a, left) and in-registry interactions between chains A–C and A–D (b, middle and right).

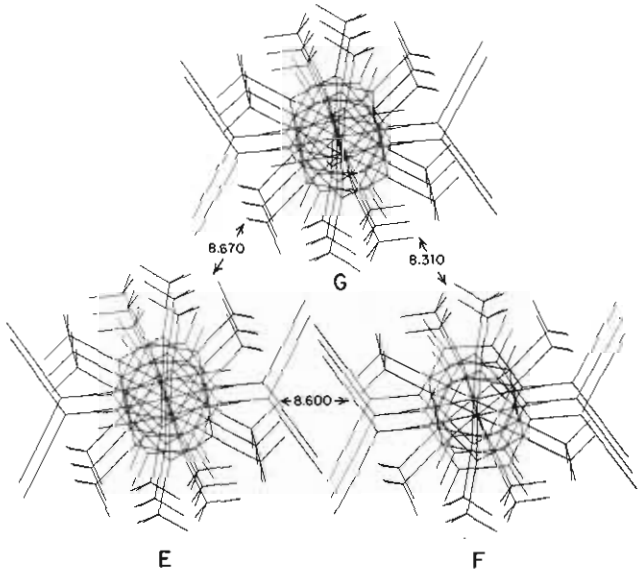

Figure 7. View normal to chains, showing the three unique chains E, F, and G for $[Fe(C_5Me_4H)_2]^{\bullet+}[TCNQ]^{\bullet-}$.

$[Fe(C_5H_5)(C_5Me_5)]^{\bullet+}$ (259 cm^{-1})[23] and suggests that the separation arising from the splitting of the e_g orbital imposed by the C_{2h} symmetry is small.

^{57}Fe Mössbauer Spectroscopy. The ^{57}Fe Mössbauer spectra of the $[Fe(C_5Me_4H)_2]^{\bullet+}$ salts contrast strongly with those of previously studied decamethylferrocenium analogues with the same basic structure type, i.e., parallel chains of alternating $\cdots D^+A^-\cdots$ cations and anions.[5b,6,8b] The isomer shift, δ (0.44 mm/s), and quadrupole coupling, ΔE (2.51 mm/s), for $Fe(C_5Me_4H)_2$ are comparable to those reported for ferrocene (δ = 0.53 mm/s; ΔE = 2.37 mm/s).[24] For $[Fe^{III}(C_5Me_4H)_2]^{\bullet+}$ the isomer shift and quadrupole coupling are typical of low-spin Fe(III) ferrocenium and confirm full charge transfer to form a monoanionic polycyanide species (Table VII).[24] There is, however, a small, but clearly resolved, quadrupole splitting effect (Figure 10) versus the sharp, relatively narrow line width ($\Gamma \sim 0.3$ mm/s) singlets exhibited by essentially all of the charge-transfer systems based on $[Fe(C_5Me_5)_2]^{\bullet+}$ studied to date.[5b,6,8b] This is most probably due to the inherently lower symmetry of C_{2h} $[Fe^{III}(C_5Me_4H)_2]^{\bullet+}$ vs D_5 $[Fe^{III}(C_5Me_5)_2]^{\bullet+}$ cations and the resulting electric field gradient. The essentially vanishing electric field gradient in ferrocenium and decamethylferrocenium relative to the neutral ferrocene analogues has been interpreted by using a molecular orbital[25] approach whose validity was confirmed by early external applied field Mössbauer spectroscopy experiments.[26]

Table VII. Mössbauer Spectroscopy Parameters for Octamethylferrocenium Species

	$Fe^{II}(C_5Me_4H)_2$		$[Fe^{III}(C_5Me_4H)_2]^{\bullet+}$-$[TCNE]^{\bullet-}$		$[Fe^{III}(C_5Me_4H)_2]^{\bullet+}$-$[TCNQ]^{\bullet-}$	
T, K	δ^a	$\Delta E^{a,b}$	δ^a	$\Delta E^{a,b}$	δ^a	$\Delta E^{a,b}$
293	0.44	2.51	0.38	0.23	0.38	0.22
78			0.47	0.30	0.45	0.29
4.8			0.47	0.31	0.45	0.29

[a] mm/s relative to natural iron foil. [b] Line widths are less than 0.3 mm/s.

The differences between the deca- and octamethylferrocene systems are highlighted in the low-temperature spectra. Figure 10 illustrates with $[Fe(C_5Me_4H)_2]^{\bullet+}[TCNE]^{\bullet-}$ the complete absence of magnetic hyperfine splitting in zero and small applied field at 4.8 K. In contrast, the decamethyl analogues with the same structure type exhibit fully resolved magnetic hyperfine splittings with internal fields of ~400 kG due to either slow paramagnetic relaxation phenomena, extended cooperative three-dimensional order, or a complex combination of both of these

(23) Miller, J. S.; Glatzhofer, D. T. Submitted for publication.
(24) Bagus, P. S.; Walgren, U. I.; Ahmolf, J. *J. Phys. Chem.* **1976**, *64*, 2324–2334. Ernst, R. D.; Wilson, D. R.; Herber, R. H. *J. Am. Chem. Soc.* **1984**, *106*, 1646–1650.
(25) Dahl, J. P.; Ballhausen, C. F. *Mat. Fys. Medd. K. Dan. Vidensk. Selsk.* **1961**, *33(5)*, 334.
(26) Collins, R. L. *J. Chem. Phys.* **1965**, *42*, 1072.

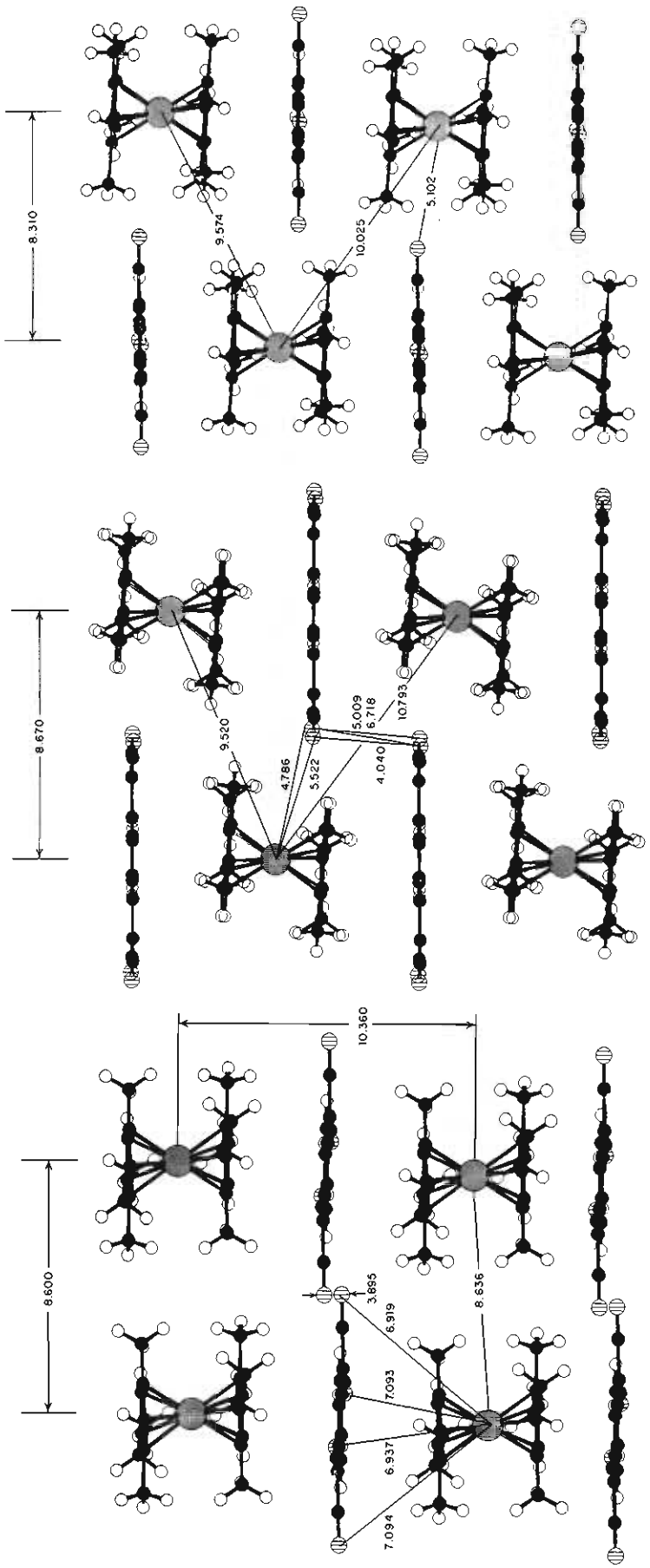

Figure 8. Out-of-registry interactions between chains E–F (a, left) and in-registry interactions between chains E–G and F–G (b, middle and right).

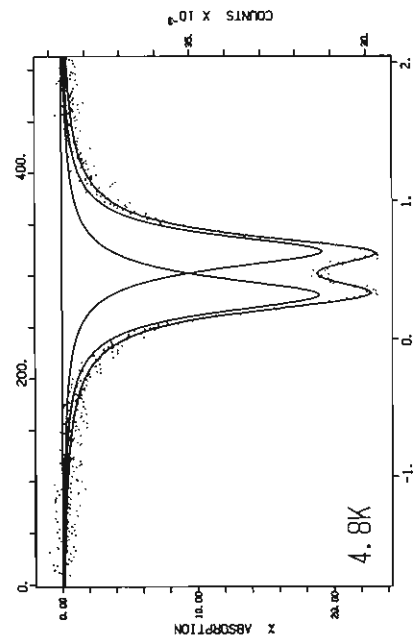

Figure 10. ^{57}Fe Mössbauer spectra for $[Fe(C_5Me_4H)_2]^{+}[TCNE]^{-}$ at 4.8 K.

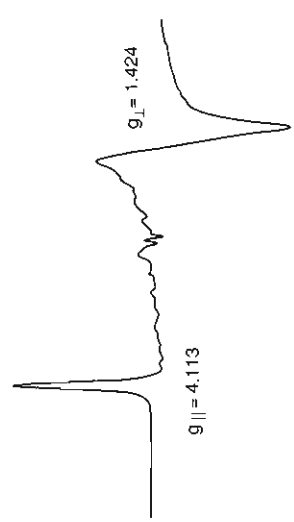

Figure 9. 7.0 K EPR spectra (CH_2Cl_2/2-methyltetrahydrofuran) of $[Fe(C_5Me_4H)_2]^{+}[BF_4]^{-}$.

Table VIII. Summary of the Magnetic Susceptibility[a] Data for $[Fe(C_5Me_4H)_2]^{+\bullet}[A]^{-\bullet}$

anion, A	μ_{eff}, μ_B	θ, K	anion, A	μ_{eff}, μ_B	θ, K
$[BF_4]^-$	3.29	+1.6	$\{C_3[C(CN)_2]_3\}^{\bullet-}$		
$[TCNE]^{\bullet-}$	3.47	−0.3	$T > 120$ K	3.97	−32.0
$[TCNQ]^{\bullet-}$	3.86	$+0.7_5$	$T < 120$ K	3.55	−1.6
$[TCNQF_4]^{\bullet-}$	3.05	−0.3	$[DDQ]^{\bullet-}$	2.70	−0.5
$[C_4(CN)_6]^{\bullet-}$	2.71	+2.7			

[a] Data for the $[TCNE]^{\bullet-}$ salts are an average of two runs, each yielding μ_{eff} of 3.13 and 3.81 μ_B.

effects. In fact, for the $[TCNE]^{\bullet-}$ and $[TCNQ]^{\bullet-}$ salts, fully consistent with the Mössbauer spectra, there is no evidence of exchange interactions or incipient ordering in the molar susceptibility data. In view of the similar structures involved, one is forced to the qualitative conclusion that the lower symmetry of the octamethylferrocenium cation alters the single-ion orbital moment properties (e.g., anisotropy and magnitude) and interion interactions, which in turn apparently have dramatic consequences for hyperfine and magnetic exchange interactions. Clearly, detailed single-crystal susceptibility and ESR studies are indispensable in this context to more fully understand the origin of what appears to be a rapidly relaxing simple paramagnetic ground state evident in this work.

Magnetic Susceptibility. The 2–320 K Faraday balance susceptibility shows that $[Fe(C_5Me_4H)_2]^{+\bullet}$ salts obeys the Curie–Weiss law, $\chi_M = C/(T - \theta)$. The effective moment μ_{eff} [$\equiv (8\chi T)^{1/2}$] and θ values are listed in Table VIII. The effective moment for a polycrystalline sample of $[Fe(C_5Me_4H)_2]^{+\bullet}[BF_4]^-$ is 3.29 μ_B. This is much greater than expected from a randomly oriented sample based on $\langle g \rangle$ (Table VI), which should yield an isotropic effective moment of 2.29 μ_B. However, a sample significantly oriented with the C_5 axis parallel to the magnetic field should result in an effective moment of 3.6 μ_B, as $g_\parallel$ is 4.11. Thus, due to the orientation variability of polycrystalline samples of these salts (as suitably large single crystals are not available to measure the magnetic anisotropy), the observed effective moments, which range from 2.71–3.97 μ_B, are consistent either one or two $S = {}^1/_2$ radical(s) per formula unit contributing to the susceptibility. The Curie–Weiss θ values are 0.5 ± 2.2 K, suggestive of very weak magnetic interactions.

For small values of θ, the exact θ obtained depends sensitively on the values utilized for the diamagnetic corrections. Using diamagnetic core corrections, χ^{core}, of -192×10^{-6} emu/mol obtained for $Fe(C_5Me_4H)_2$ and separately measured χ^{core} values of -60×10^{-6} emu/mol for TCNE and -98×10^{-6} emu/mol for TCNQ, one obtains θ values of −0.3 and +0.7 K for the $[TCNE]^{\bullet-}$ and $[TCNQ]^{\bullet-}$ salts, respectively. An alternate approach was used for these salts, i.e., extrapolating χ vs T^{-1} to infinite temperature. The values for χ^{core} obtained, -237×10^{-6} and -286×10^{-6} emu/mol for the $[TCNE]^{\bullet-}$ and $[TCNQ]^{\bullet-}$ salts, respectively, resulted in θ's of +7 and +4.5 K for the $[TCNE]^{\bullet-}$ and $[TCNQ]^{\bullet-}$ salts, respectively. These latter values are the more appropriate ones, since the effective moment versus temperature plots for these two systems show a significant ferromagnetic interaction in these materials.

The $\{C_3[C(CN)_2]_3\}^{\bullet-}$ salt is anomalous, as a change in $\chi(T)$ is evident at ~120 K (Figure 11). Above 120 K the reciprocal magnetic susceptibility obeys the Curie-Weiss expression with μ_{eff} of 3.97 μ_B and θ = −32 K; whereas below 120 K the data obeys the Curie-Weiss expression with μ_{eff} of 3.55 μ_B and θ = −1.6 K. The low-temperature values are comparable to the other octamethylferrocenium salts; however, the high-temperature values suggest a higher moment state with substantial antiferromagnetic coupling. Crystallographic data should provide insight into this phenomena, but the lack of suitable crystals has hampered continued studies in this area.

Due to the structural characterization of the $[TCNE]^{\bullet-}$ and $[TCNQ]^{\bullet-}$ salts a more detailed interpretation of the susceptibility data can be made. Both of these salts possess isolated $S = {}^1/_2$ anions; thus, the spins from both the cations and anions contribute to the susceptibility. For the $[TCNE]^{\bullet-}$ salt the expected isotropic

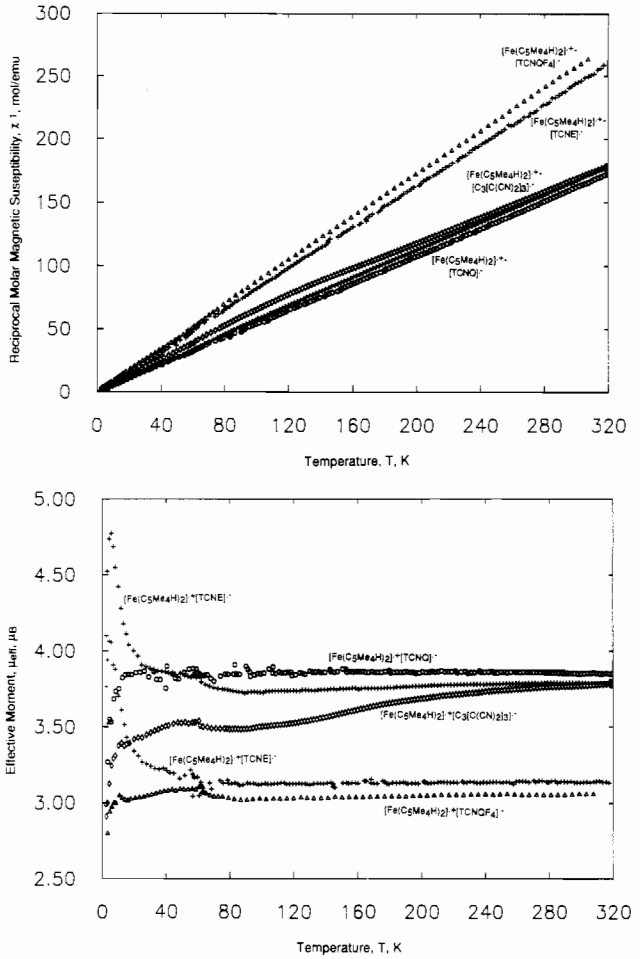

Figure 11. Inverse molar magnetic susceptibility (a, top) and effective moment (b, bottom) of $[Fe(C_5Me_4H)_2]^{+\bullet}[A]^{-\bullet}$ [A = TCNE (+), TCNQ (○), $TCNQF_4$ (△), $C_3[C(CN)_2]_3$ (◇)] as a function of temperature.

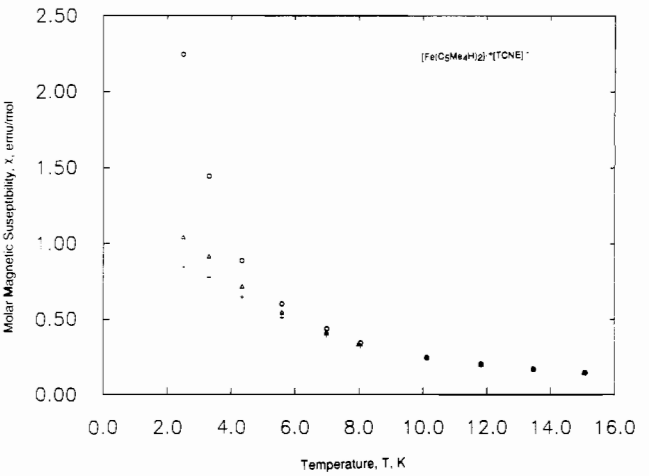

Figure 12. Magnetic susceptibility as a function of temperature at 5.25 (○), 15.85 (△), and 19.5 (+) kG applied field for two samples of $[Fe(C_5Me_4H)_2]^{+\bullet}[TCNE]^{\bullet-}$.

moment is 2.78 μ_B whereas a sample oriented parallel to the chain direction would have a limiting moment of 3.96 μ_B. Moments from two samples of the $[TCNE]^{\bullet-}$ salt are 3.13 and 3.81 μ_B, which are bracketed by these limiting values, and as evidenced by the same temperature dependencies, suggest the samples are oriented differently. The data presented for the $[TCNQ]^{\bullet-}$ salt is similar to that of the higher moment orientation of the $[TCNE]^{\bullet-}$ salt; i.e., μ_{eff} = 3.86 μ_B.

For the $[Fe(C_5Me_4H)_2]^{+\bullet}[TCNE]^{\bullet-}$ salt the reciprocal susceptibility deviates from the Curie–Weiss law below ~5 K and the molar susceptibility exhibits a marked field dependence (Figure 12). Magnetization data were obtained as a function of applied

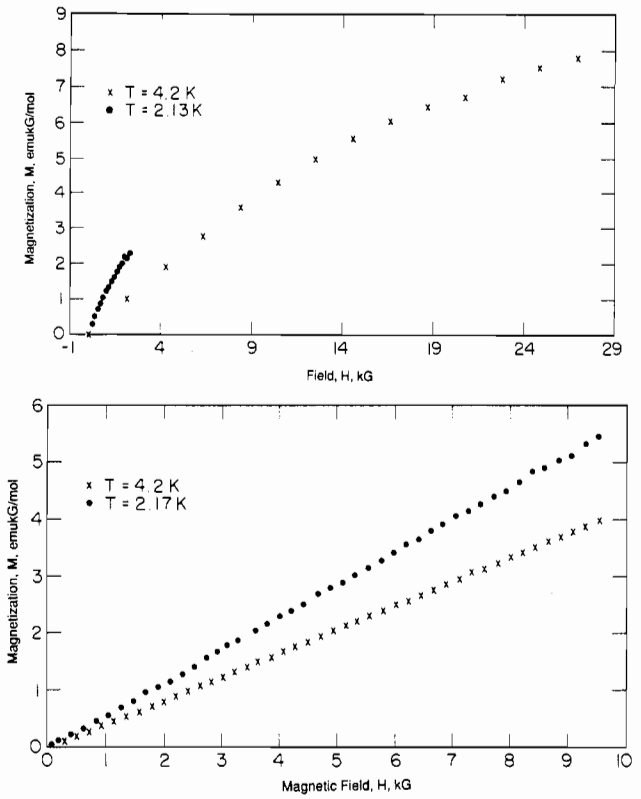

Figure 13. Magnetization as a function of applied field at 2.13 and 4.2 K for $[Fe(C_5Me_4H)_2]^{\bullet+}[TCNE]^{\bullet-}$ (a, top) and at 2.17 and 4.2 K for $[Fe(C_5Me_4H)_2]^{\bullet+}[TCNQ]^{\bullet-}$ (b, bottom).

field at 2.1 and 4.2 K (Figure 13a). Hysteresis loops characteristic of a bulk ferromagnet were not observed, demonstrating the absence of three-dimensional ferromagnetic ordering. However, magnetization as a function of the applied field rises faster than the Brillouin function both at 2.1 and 4.2 K, suggesting ferromagnetic interactions.

For the $[Fe(C_5Me_4H)_2]^{\bullet+}[TCNQ]^{\bullet-}$ salt, the reciprocal susceptibility and effective moment as a function of temperature are shown in Figure 11. Although not as dramatic as for $[Fe(C_5Me_4H)_2]^{\bullet+}[TCNE]^{\bullet-}$, the effective moment rises with decreasing temperature up to ~10 K, suggesting that the primary interaction along the chain is ferromagnetic. Below 10 K, however, there is a suppression in the effective moment suggestive of weaker antiferromagnetic interactions between chains (vide infra).

The magnetization at 2.2 and 4.2 K as a function of applied field is shown in Figure 13b and is essentially linear. The increase in magnetization in going from 4.2 to 2.2 K is less than that expected for a simple Curie law. At 2.2 K there is a small anomaly in $M(H)$ at ~3 kG. Sufficiently large single crystals are necessary to more completely characterize this effect.

Conclusion

The absence of three-dimensional ferromagnetic or antiferromagnetic ordering to 2.2 K in either $[Fe(C_5Me_4H)_2]^{\bullet+}[TCNE]^{\bullet-}$ or $[Fe(C_5Me_4H)_2]^{\bullet+}[TCNQ]^{\bullet-}$ with respect to $[Fe(C_5Me_5)_2]^{\bullet+}[A]^{\bullet-}$ (A = TCNE, TCNQ) is in accord with the ^{57}Fe Mössbauer data, which only shows nuclear quadrupole splitting for the $[Fe(C_5Me_4H)_2]^{\bullet+}$ salts. The lack of magnetic ordering may be due to poorer interionic overlap within and between the chains leading to substantially weaker magnetic coupling for the $[Fe(C_5Me_4H)_2]^{\bullet+}$ structures with respect to the analogous $[Fe(C_5Me_5)_2]^{\bullet+}$ structures. This would be expected to suppress the spin-ordering temperature with respect to that observed for $[Fe(C_5Me_5)_2]^{\bullet+}[A]^{\bullet-}$. Alternatively, due to the overall C_{2h} symmetry the $[Fe(C_5Me_4H)_2]^{2+}$ charge-transfer excited state may be a singlet state, not a triplet as expected for $[Fe(C_5Me_5)_2]$[23]. The admixture of a singlet, not a triplet, charge-transfer excited state should lead to antiferromagnetic, not ferromagnetic, coupling.[5,11] At low temperatures when $k_BT < 2\delta$ {the e_{2g} ($d_{x^2-y^2}/d_{xy}$) splitting introduced by the lowering of the symmetry for $[Fe(C_5Me_4H)_2]^{\bullet+}$}, the singlet, not triplet, charge-transfer state may dominate, leading to a crossover from ferromagnetic to antiferromagnetic exchange. The magnitude of the exchange interaction may also decrease at low temperature as now only one orbital (i.e., $d_{x^2-y^2}$ or d_{xy}) is involved with the overlap with its neighbors.

Acknowledgment. A.C., D.T.G, A.J.E. and J.S.M gratefully acknowledge support from Department of Energy Division of Materials Science Grant No. DE-FG02-86ER45271.A000. W.M.R. gratefully acknowledges support from NSF DMR Solid State Chemistry Program Grant No. 8313710. We also appreciate the stimulating discussions with D. A. Dixon, J. R. Morton, and M. D. Ward, the synthetic assistance supplied by D. Wipf, the Faraday susceptibility data taken by R. S. McLean, and the cyclic voltammetry data obtained by E. Delawski and M. D. Ward (Du Pont CR&DD).

Registry No. TCNE, 670-54-2; TCNQ, 1518-16-7; DDQ, 84-58-2; $TCNQF_4$, 29261-33-4; n-$C_4(CN)_6$, 5104-27-8; $Fe(C_5Me_4H)_2$, 59568-28-4; $[Fe(C_5Me_4H)_2]^{\bullet+}[BF_4]^-$, 121192-65-2; $[Fe(C_5Me_4H)_2]^{\bullet+}[TCNE]^{\bullet-}$, 120557-41-7; $[Fe(C_5Me_4H)_2]^{\bullet+}[TCNQ]^{\bullet-}$, 120551-18-0; $[Fe(C_5Me_4H)_2]^{\bullet+}[n\text{-}C_4(CN)_6]^{\bullet-}$, 121192-66-3; $[Fe(C_5Me_4H)_2]^{\bullet+}[DDQ]^{\bullet-}$, 121210-58-0; $[Fe(C_5Me_4H)_2]^{\bullet+}[TCNQF_4]^{\bullet-}$, 121192-67-4; $[Fe(C_5Me_4H)_2]^{\bullet+}\{C_3[C(CN)_2]_3\}^{\bullet-}$, 121192-68-5; tetra-$n$-butylammonium tris(dicyanomethylene)cyclopropanide, 58608-56-3.

Supplementary Material Available: Tables S1–S7, listing crystallographic data, bond angles, least-squares planes, and anisotropic thermal parameters for $[Fe(C_5Me_5)_2]^{\bullet+}[A]^{\bullet-}$ (A = TCNQ, TCNE) (9 pages); Tables S8 and S9, listing calculated and observed structure factors (18 pages). Ordering information is given on any current masthead page.